NANO EXPRESS

Electrically tunable solid-state silicon nanopore ion filter

**Julien Vidal · Maria E. Gracheva ·
Jean-Pierre Leburton**

Abstract We show that a nanopore in a silicon membrane connected to a voltage source can be used as an electrically tunable ion filter. By applying a voltage between the heavily doped semiconductor and the electrolyte, it is possible to invert the ion population inside the nanopore and vary the conductance for both cations and anions in order to achieve selective conduction of ions even in the presence of significant surface charges in the membrane. Our model based on the solution of the Poisson equation and linear transport theory indicates that in narrow nanopores substantial gain can be achieved by controlling electrically the width of the charge double layer.

Keywords Ion channels · Artificial nanopore · Silicon materials · Nanofluidics

Introduction

Ion channels have been extensively studied during the past years for their essential role in cell biology. Their most important properties are the regulation of ion flow and their ion selectivity [1, 2] as they allow only certain type of ions to cross through cell membranes

J. Vidal · J.-P. Leburton (✉)
Department of Electrical and Computer Engineering,
University of Illinois at Urbana-Champaign, Urbana
IL 61801, USA
e-mail: jleburto@uiuc.edu

J. Vidal · M. E. Gracheva · J.-P. Leburton
Beckman Institute for Advanced Science and Technology,
University of Illinois at Urbana-Champaign, Urbana, IL
61801, USA

depending on the cell ion concentration and the membrane surface charge. In this process the cell controls the flow of ions by a biological gate at the bottom of the channel thereby opening and closing a molecular sensor. This sensor reacts to change in concentration of certain types of ions and other biological signals. However, biological sensors, due to their finite size, their bio-chemical stability and low noise characteristics are restricted to well defined thermal, chemical, mechanical and electrical conditions [3]. In the last couples of years solid-state nanopores made of silicon or compound silicon materials have been proposed as subsitutes to biological channels for their versatility and physical robustness [3–5]. The nanopores are manufactured using conventional semi-conductor processing techniques, starting with a 200 mm Silicon wafer with a silicon layer 20 nm thick [6]. A membrane is formed by creating a through-wafer via using optical lithography in conjunction with ion and wet chemical etching on sacrificial layers. A nanopore of very small diameter ($\approx$1 nm) can be produced in the membrane using a tightly focused, high-energy electron beam. The presence of surface charge on the membrane modulated by the voltage applied to the semiconductor creates double layer according to the well-known Poisson–Boltzmann equation. Because the electrolyte Debye length is comparable to the pore radius (e.g., for $C = 1$ M, $\lambda_D = 3$ Å), the cylindrical double layer in the solution occupies a significant volume of the nanopore and surface charge-controlled ion transport arises. In their seminal work, Nishizawa et al. have shown that membranes containing cylindrical metallic nanotubules exhibit selective ion transport due to the potentiostatically charge on the wall of the nanotubules [7]. Meanwhile ionic

transistors and diode behavior devices [8–11], DNA sequencing devices [6] have been proposed. By forming electrical contacts on the solid-state membrane, it is possible to use the membrane as a capacitor, and modulate, even offset the surface charge on the synthetic nanopore in order to control the ion concentration inside the nanopore. Therefore by inducing a potential difference between the membrane and the electrolyte, the respective ion concentrations can be tuned to desirable values, thereby mimicking the behavior of ions channels to regulate ion flow. The advantages of such a system over other proposals for ion filtering are its design simplicity compared to more complicated device structures [12, 13], the use of well established silicon nano-technology for electrical reliability, and its electrical tunability in contrast to devices with permanent and unalterable surface charges [8]. In this paper, we show the electrically tunable filtering capability of silicon nanopores by using an approach based on the self consistent solution of a 3D Poisson's equation and the linear transport theory for which we propose a phenomenologic model for ion mobility in nanopore which is consistent with experimental results. We consider realistic silicon nanopores structures with double cone shape as resulting from electron beam fabrication techniques, and take into account the presence of surface charges inside the nanopore membrane.

Device structure

We consider a Si-membrane containing the nanopore immersed in an electrolytic transport bi-cell. The cells on each side of the membrane contain a volume of KCl electrolyte and an electrode positioned at 1 mm from the membrane. Figure 1 illustrates schematically the

solid-state nanopore device where a potential difference between the electrodes in each cell drives the ion current through the nanopore. The solid-state membrane is very thin (≈ 10 nm) and made of heavily doped polysilicon. A nanopore of diameter smaller or equal to 2 nm is etched through the membrane using a tightly focused, high-energy electron beam to sputter atoms [14–16]. As a consequence, the nanopore has the shape of two inverted cones. The principle of operation is simple: by applying a positive (negative) potential difference between the poly-silicon and the electrolyte, negative (positive) ions are attracted into the nanopore and positive (negative) ions are repelled and thereby modulating selectively the conductance of the respective ions. Details of the structure and its fabrication can be found in Ref. [16].

3D Self-consistent model

We define our simulation volume by focusing on the pore region which is the active region of the device for which a schematic cross-section of the idealized device is shown on Fig. 1. We denote several specific coordinates (Y_c, Y_1), for which the mobility profiles will be displayed in subsequent figures. The system under investigation consists of a thin layer of heavily doped n^+-Si with a doping concentration $N_d^+ = 2 \times 10^{20}$ cm^{-3} surrounded by a thin 2 Å layer of negative charge with volume density $N_{surface} = 2 \times 10^{21}$ cm^{-3} as a result of the etching process [4]. The electrolyte charge originates from K$^+$ and Cl$^-$ ions. At room temperature the molecules are fully ionized. Recently, Eisenberg et al. investigating transport in ion channels using semiconductor device formalism showed that their treatment is fully reliable to account for experimental results [17]. Therefore in our approach, we consider the electrolyte
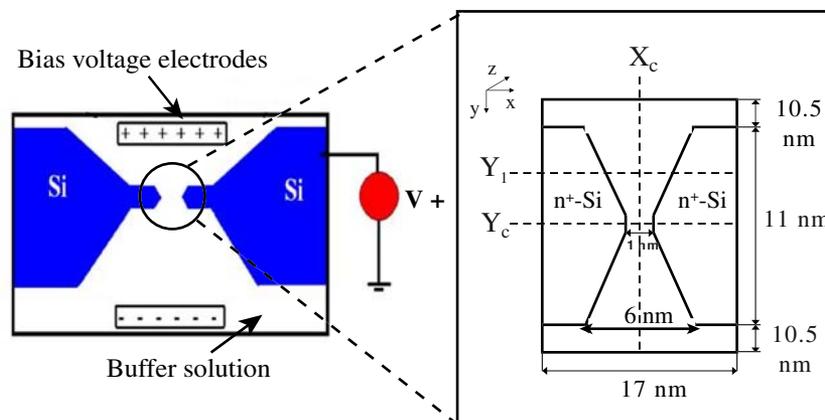
Fig. 1 Schematic of the device geometry: xy cross-section through the center of the device. The drawing is not to scale

as a continuum and use the semiconductor equation formalism to model its electrical properties as well as those of the silicon membrane. Hence, the system consists of two material regions defined by their relative permittivity, i.e., ϵ_{Si} = 11.7 for the Si-membrane and $\epsilon_{solution}$ = 78 for the solution. Although the local permittivity can vary from 78 to 1 depending whether the water is totally excluded or not of the nanopore in this analysis, we neglect any spatial variation of $\epsilon_{solution}$. In this framework, the KCl solution is assumed to be an intrinsic semiconductor.[1] In the presence of an electrostatic potential ϕ (**r**), the ion concentrations [Cl⁻] (**r**) and [K⁺] (**r**) obey Boltzmann Statistics:

$$[K^+](\mathbf{r}) = [K^+]_0 \exp\left[\frac{q\phi(\mathbf{r})}{k_B T}\right] \qquad (1)$$

$$[Cl^-](\mathbf{r}) = [Cl^-]_0 \exp\left[-\frac{q\phi(\mathbf{r})}{k_B T}\right], \qquad (2)$$

where $[K^+]_0$ and $[Cl^-]_0$ are the equilibrium concentrations, T the temperature and k_B the Boltzmann constant. The net ionic charge density in the solution is:

$$\rho_{solution} = q\{[K^+](\mathbf{r}) - [Cl^-](\mathbf{r})\}. \qquad (3)$$

In the Si-layer, the carriers are degenerate, and their distributions follow the Fermi–Dirac distribution. The local density of charges in the semiconductor region is given by:

$$\rho_{solid-state}(\mathbf{r}) = q\{N_d^+(\mathbf{r}) - N_s^-(\mathbf{r}) + p(\mathbf{r}) - n(\mathbf{r})\}, \qquad (4)$$

where N_d^+ is the fully ionized donor density and N_s^- is the fixed surface charge.

Poisson's equation,

$$\vec{\nabla} \cdot \left(\epsilon(\mathbf{r}) \; \vec{\nabla}\phi(\mathbf{r})\right) = -\rho(\mathbf{r}), \qquad (5)$$

is solved self-consistently by a multigrid approach on the whole device under investigation [6]. The grid spacing ranges from 4 Å to 0.5 Å as to be less than the Debye length. We assume Dirichlet boundary conditions on top and bottom bias gate region and Neumann boundary condition elsewhere. With no applied voltage, Fermi level in the whole device are

set to zero, but when a voltage V_{SE} is applied between the semiconductor and the electrolyte, their respective quasi-fermi levels $E_{f\ silicon}$ and $E_{f\ electrolyte}$ are split according to:

$$E_{f\ silicon} - E_{f\ electrolyte} = -qV_{SE}. \qquad (6)$$

Therefore, we can investigate both the semiconductor region and the electrolyte region and their mutual interaction under external bias. Figure 2a and b display both cation and anion concentrations for $V_0 = V_{SE} = 0$. Figure 2c and d show the corresponding potential profiles along respectively Y_c (red curve) and Y_1 (blue curve). On Fig. 2a, one notices the depletion layer (positive N_D^+ charge) in the n^+-region running along the semiconductor membrane, which inverts the ionic population (Cl⁻ dominant) along the slanted part of the nanopore (dark red in Fig. 2a and yellow in Fig. 2b). At the tip and the wide opening of the pore, cations are attracted close to the semiconductor surface due to the negative surface charge (dark red in Fig. 2b), while anions are strongly repelled (green and yellow in Fig. 2a). The potential variation along the Y-direction is relatively weak because of the strong screening provided by the high ion concentration. It is sufficient, however to distinguish inhomogeneous anion and cation distributions in the nanopore. On Fig. 2c the potential minimum at the pore center followed by two maxima is due to the particular double conic shape of the pore. On Fig. 2d the smaller variation is at Y_c, in the pore constriction, as expected.

Recent experimental data [4] indicate the ion conductance decreases with pore radii due to the surface roughness, which implies ion mobilities vary spatially inside the nanopore. We use a phenomenological model for the mobility of each type of ions to ensure it vanishes on the nanopore wall i.e.,

$$\mu_{a,c}(r) = \mu_{a_0,c_0}\left\{1 - \exp\left[\frac{-|r - R(y)|^{\gamma_{a,c}}}{\delta_{a,c}^{\gamma_{a,c}}}\right]\right\}, \qquad (7)$$

Here, the subscripts a and c refer to anions and cations, respectively, μ_{a_0,c_0} is the ionic bulk mobility, r is the radial distance from the center of the pore, $R(y)$ is the pore radius at ordinate y, δ and γ are two fitting parameters that account for the decay of the mobility near the pore wall. We assume δ and γ are the same for both Cl⁻ and K⁺ because the bulk mobility for cations and anions is pratically the same i.e., $\mu_{a_0} = 7.91 \times 10^{-8}\ m^2\ V^{-1}\ s^{-1}$, $\mu_{c_0} = 7.12 \times 10^{-8}\ m^2\ V^{-1}\ s^{-1}$. Specifically:

---

[1] We assign virtual solid states parameters as an effective band gap E_{geff}, a virtual density of states, a virtual effective mass and a conduction band offset between the semiconductor and the electrolyte. We define these parameters in the same way as defined in solid state theory [18, 19].
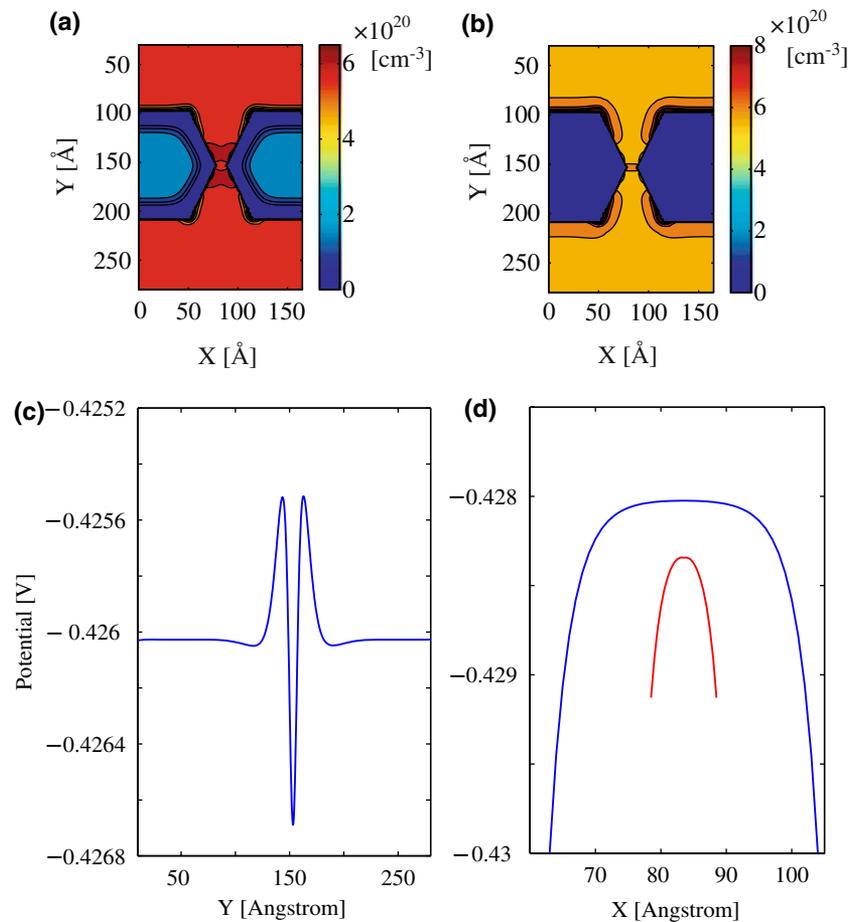
Fig. 2 (**a**) and (**b**) Contour plot of ion concentration in the electrolyte and mobile charges in the membrane for a surface charge of –0.064 C m^{-2}, a doping concentration $N_\mathrm{d}^+ = 2 \times 10^{20}$ cm^{-3} and an ion concentration of 1 M: (**a**) anion and electron concentrations, (**b**) cation and hole concentrations. (**c**) and (**d**): Potential profile at X_c along the Y-direction (**c**); and at Y_c (**d** red curve) and Y_1 (**d** blue curve) along the X-direction

– δ is a characteristic length that accounts for the reduction of ion mobility due to the presence of the solid-state surface in the nanopore. Hence, for $r = 0$ and $R = 5$ Å, if we choose $\gamma = 4$ and $\delta = 8$ Å, $\mu_\mathrm{a,c} \approx \mu_\mathrm{a_0,c_0} \left(\frac{R}{\delta}\right)^\gamma$ and the mobility is reduced by 85% compared with the bulk values, which is consistent with existing data [20, 21]. Figure 3a displays the mobility profile along the Y_c direction (Fig. 1) in the narrowest region of the device as δ is varied. It is seen that as δ increases $\mu_\mathrm{a,c}(r = 0)$ decreases.

– γ accounts for the rate of decrease of the counterion mobility near the surface. Hence, for $\mid r - R \mid = \epsilon \approx 0$, $\frac{\mathrm{d}\mu_\mathrm{a,c}}{\mathrm{d}r} \propto \epsilon^{2\gamma-1}$ and $\mu_\mathrm{a,c} \propto \epsilon^\gamma$. Figure 3b shows the mobility profile along the Y_1 direction (Fig. 1) for different values of γ. It is seen that the mobility variation is smoother in the vicinity surface as γ increases (i.e., $\frac{\mathrm{d}\mu_\mathrm{a,c}}{\mathrm{d}r}$ is small).

A more refined mobility model based on molecular dynamics would generalize this approximation but is beyond the purpose of this work. We model the potential variation through the nanopore with the following analytical expression, which has been shown to be valid from molecular dynamics in nanopore [22]:

$$V(y) = \frac{V_0}{\pi} \tan^{-1}(y/L_\mathrm{eff}), \qquad (8)$$

where V_0 is the external voltage across the device driving the ions through the nanopore and L_eff is a characteristic length (not the channel length) so that the potential achieves its electrode values at $y = [-L_y/2, L_y/2]$ where L_y is the channel length, with non-zero electric field at the electrodes. We made the important approximation that reservoir resistance is negligible in comparison with nanopore resistance and the potential in the reservoir is mostly constant.
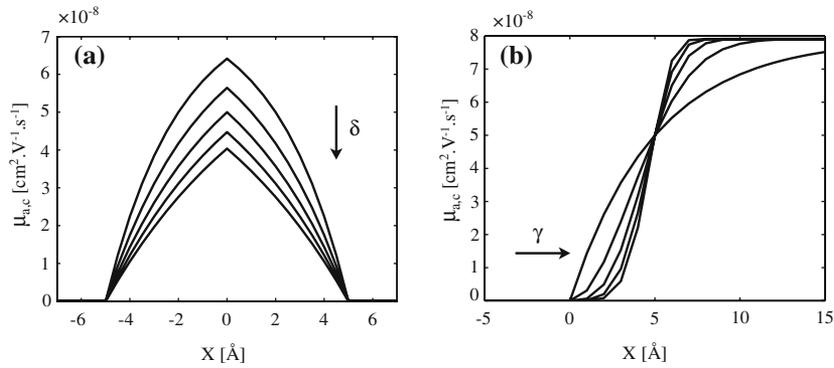
Fig. 3 Mobility profiles at different positions in the channel: (**a**) along the center plane of the device Y_c for different δ varying by unitary step from $\delta = 3$ Å to $\delta = 7$ Å and $\gamma = 1$ (**b**) along Y_1 near the wall for γ varying by unitary step from $\gamma = 1$ to $\gamma = 5$ and $\delta = 5$

Considering both anion density current and cation density current and neglecting the diffusion current, the current density for each ion type is given by

$$J_a = q\mu_a a \nabla\phi, \tag{9}$$

$$J_c = q\mu_c c \nabla\phi, \tag{10}$$

$$J = J_a + J_c, \tag{11}$$

where μ_a and μ_c are the anion and cation mobility, respectively. Assuming no recombination inside the pore, we have

$$\nabla J_{a,c} = 0, \tag{12}$$

which by using the divergence theorem, implies that the current is constant through the nanopore. Due to the one dimensional nature of the external potential (8), this condition (12) is not fully satisfied.[2] Therefore, we spatially average the current through the nanopore to eliminate the slight J-variations due to the slanted geometry of the nanopore:

$$\langle I_{a,c}\rangle = \frac{1}{L}\int_{L/2}^{-L/2} dy \iint_{S(y)} J_{a,c}(\mathbf{r})dS, \tag{13}$$

Here L is the length of the pore and $S(y)$ is the nanopore cross section at ordinate y. In this context, we define each ion conductance in the nanopore as

$$G_{a,c} = \langle I_{a,c}\rangle/V_0. \tag{14}$$

_____
[2] A full 3D self consistent approach with sufficient spatial resolution in the nanopore is presently computationally prohibitive.

Results and discussion

At zero electrolyte-membrane bias V_{SE}, there is predominance of cations inside the pore due to the presence of the negative charge on the nanopore wall irrespectively of the pore size and electrolyte concentration. When varying V_{SE}, the ion concentration inside the pore changes according to the voltage magnitude and its polarity. Figure 4 shows the average volumic concentrations for both K$_+$ and Cl$_–$ ions defined as

$$n_{avg} = \frac{\iiint n(\mathbf{r})d\mathbf{r}}{V_{pore}}, \tag{15}$$

for various pore shapes, surface charges on the semiconductor and electrolyte concentrations as functions of V_{SE} at $V_0 = 0$. Here V_{pore} is the volume of water inside the pore and $n(\mathbf{r})$ the ion concentration at position $\mathbf{r}$. Equation 15 directly provides the number of ions inside the pore since V_{pore} is only dependent on the nanopore geometry. We also denote the cation concentration gain as $\beta_c^+ = \frac{[K^+]}{[Cl^-]}$ and the cation conductance gain as $\beta_G^+ = \frac{G_c}{G_a}$ (The corresponding anion gains are the inverse of these quantities). For all four cases, the respective ion concentrations change monotonically with applied voltage. Hence, when the voltage V_{SE} is sufficiently negative, cations are predominant in the nanopore, while at high positive voltages, the situation is reversed and anions are the predominant species. We define the turning voltage V_T^c as

$$V_T^c = V_{SE}(n_{avg}^a = n_{avg}^c), \tag{16}$$

i.e. when the average volumic concentrations for cations and anions equalize. In the case of an ideal
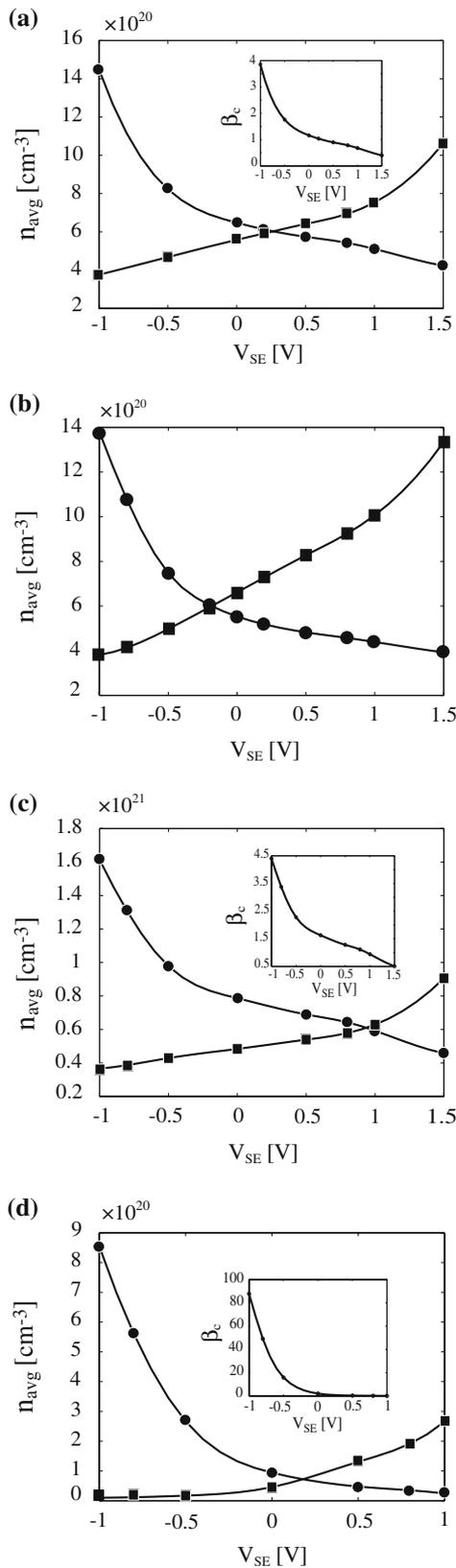
◀ **Fig. 4** Main panels: Average volumic concentration of K^+ (circle) and Cl^- (square) and insets: β_c, versus voltage applied: (**a**) for a surface charge of -0.064 C m^{-2}, ion concentration of 1 M, (**b**) for a surface charge of -0.064 C m^{-2}, a doping concentration $N_d = 5 \times 10^{20}$ cm^{-3} and ion concentration of 1 M, (**c**) for a surface charge of -0.096 C m^{-2} and ion concentration of 1 M, (**d**) for a surface charge of -0.064 C m^{-2} and ion concentration of 0.1 M

nanopore without surface and bulk charge, the turning voltage V_T^c is zero, but for a semiconductor membrane, V_T^c depends on the surface charge, semiconductor doping concentration, and nanopore shape. For a surface charge of -0.064 C m^{-2} (Fig. 4a), V_T^c is around 0.25 V in our structure. Figure 4b shows the ion concentration profiles for a membrane with a higher donor concentration, which results in a larger depletion charge, repelling cations in the pore and shifting V_T^c to negative V_{SE} values. However, the quantitative behavior of the concentration curves remains roughly the same, varying within similar values for the same voltage range. Therefore the cation concentration gain β_c^+ has pratically the same profile as Fig. 4a inset. Changes in the surface charge do not modify qualitatively this behavior but tends to shift V_T^c towards positive values as the V_{SE} potential (applied to the semiconductor) is now screened by the large negative surface charge (Fig. 4c). Lowering the electrolyte concentration improves the ion selectivity of the pore: indeed, greater concentration gain β_c^+ is achieved for lower electrolyte concentrations (Fig. 4 insets). This effect is due to a longer Debye length for which the double layers on each side of the nanopore overlap over the whole inner volume, while for higher electrolyte concentrations resulting in a smaller Debye length, double layer overlap occurs only in the narrowest region of the pore. One also notices that the average volumic concentration is never zero for both types of ions because of edge effects, i.e. at both extremities of the nanopore, where the influence of the voltage between the electrolyte and the semiconductor is weak and where both the anions and cations concentrations in these nanopore regions rapidly reach bulk values. Figure 5 show the cation and anion conductance variations as a function of V_{SE} for the same parameters as in Fig. 4. As for the ion concentration variations versus V_{SE}, we can define a conductance turning voltage $V_T^G = V_{SE}(G_a = G_c)$, for which the anion conductance and the cation conductance equalize. As seen in Fig. 5a, for a surface charge of -0.064 C m^{-2}, $V_T^G \approx -0.35$ V which is different from V_T^c for the same conditions. This difference is mainly due to the mobility profiles which do not coincide with the ion concentration profiles
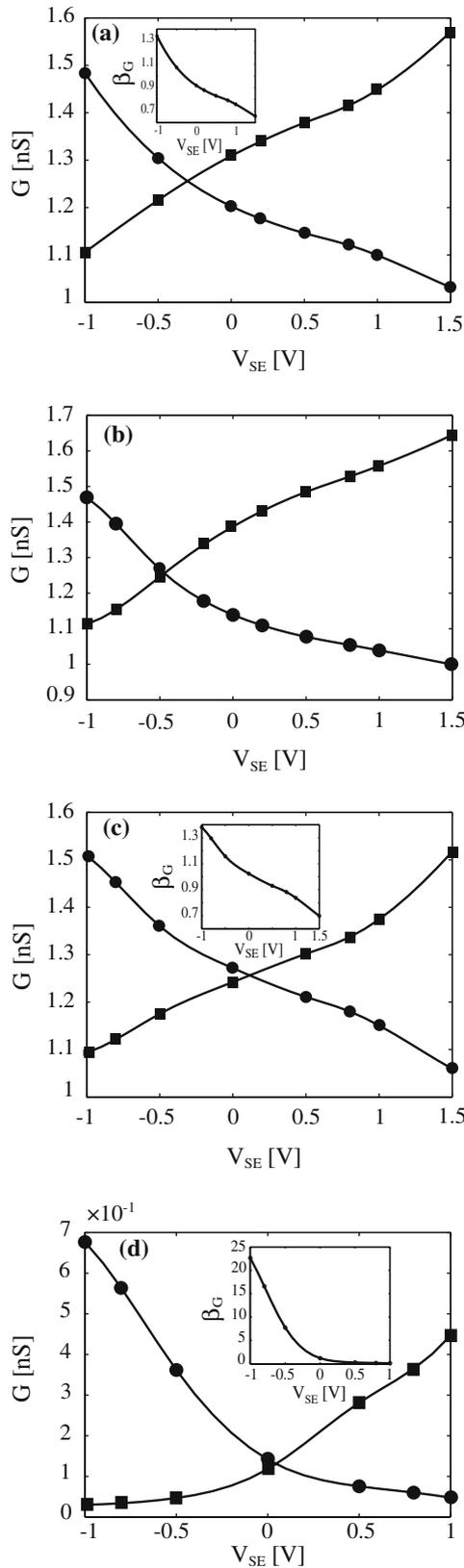
◀ **Fig. 5** Main panels: Conductance of K$^+$ (circle) and Cl$^-$ (square) ions and insets: β_G versus voltage applied: (**a**) for a surface charge of –0.064 C m^{-2}, an ion concentration of 1 M, (**b**) for a surface charge of –0.064 C m^{-2}, a doping concentration $N_d^+ = 5 \times 10^{20}$ cm^{-3} and ion concentration of 1 M, (**c**) for a surface charge of –0.096 C m^{-2} and ion concentration of 1 M, (**d**) for a surface charge of –0.064 C m^{-2} and ion concentration of 0.1 M

inside the nanopore. Furthermore, cation bulk mobility is 10% smaller than the anion one, also resulting in a shift of V_T^G towards negative voltage. High doping concentration in the n$^+$-membrane shifts V_T^G towards negative values because the positive charges in the depletion layer overcomes the influence of the negative surface charge (Fig. 5b). We introduce the filter selectivity defined as

$$S = \frac{|G_c - G_a|}{G_c + G_a} = \left| \frac{\beta_G - 1}{\beta_G + 1} \right|.$$

When $S \approx 1$, either G_a or G_c is zero, and so the nanopore allows only one type of ions to cross the membrane as in a perfect filter. If $S \approx 0$, then $G_c \approx G_a$ and the nanopore does not discriminate between both types of ions, and behaves like a passive channel between two reservoirs. For both Fig. 5a and b, a conductance gain $\beta_G^+ \approx 1.3$ and a maximum selectivity $S_{max} \approx 0.15$ are achieved. Such a low efficiency can be explained by side effects at the opening regions of the pore where ions are not affected by the voltage differences applied between the semiconductor and the electrolyte and ions behave as in a bulk solution. Figure 5c displays the conductance curves for higher surface charge (–0.096 C m^{-2}), resulting in a V_T^G increase due to the negative surface charge that tends to attract more cations than anions in the nanopore. Both gain and selectivity remains the same for increasing surface charges. For a lower concentration [K$^+$]$_0$ = [Cl$^-$]$_0$ = 0.1 M (Fig. 5d), two phenomena arise: first the conductance for both cations and anions decreases due to the fact that less ions are present in the solution; second, greater conductance gain $\beta_G^+ \approx$ 23 and a maximum selectivity $S_{max} \approx 0.92$ are achieved, due to the vanishing edge effects. Indeed, the Debye length λ_D is now comparable to the smallest diameter in our device (≈ 10 Å), and then double layer overlap occurs in most of the nanopore and not only at its bottle neck. Hence, by decreasing the electrolyte concentration or the nanopore diameter of the nanopore, the selectivity of the ion filter is greatly improved.

Conclusion

Owing to their electrical versatility semiconductor membranes are relatively well suited for modulating electrically the ionic conductance of electrolytic solutions through an artificial nanopore. Our model based on an all-semiconductor formalism incorporating electrolyte and solid-state electronics has provided physical insight into the different factors influencing the nanopore electrostatics for ion filtering applications. Specifically the competition between depletion charges and surface charges, in addition to the conductive properties of doped semiconductor materials accounts for the electrical tunability of the membrane. Although of finite filtering capability, significant gains in selectivity in terms of ionic concentration and conductance are obtained, especially for low molar concentrations of the electrolyte. One of the main advantages of this filtering scheme is its material property, which relies on semiconductor technology with its ability for miniaturization and electronic integration. Therefore, for large filtering gains, the possibility of integrating several individual nanopore membranes into a cascade device with finite but non-unity gain at each stage is anticipated.

References

1. A.L. Hodgson, A.F. Huxley, B. Katz, J. Physiol. **116**, 424 (1952)
2. D.A. Doyle, J.M. Cabral, R.A. Ofuetzner, A. Kuo, J.M. Gulbis, S.L. Cohen, B.T. Chait, R. MacKinnon, Science **280**, 69 (1998)
3. J. Li, M. Gershow, D. Stein, E. Brandin, J.A. Golovchenko, Nat Mater **2**, 611 (2003)
4. C. Ho, R. Qiao, J.B. Heng, A. Chatterjee, R.J. Timp, N.R. Aluru, G. Timp, Proc. Natl. Acad. Sci. **102**, 10445 (2005)
5. J.B. Heng, C. Ho, T. Kim, R. Timp, A. Aksimentiev, Y.V. Grinkova, S. Sligar, T. Sprosch, K. Schulten, G. Timp, Biophys. J. **87**, 2905 (2004)
6. M.E. Gracheva, A. Xiong, J.P. Leburton, A. Aksimentiev, K. Schulten, G. Timp, Nanotechnology **17**, 622 (2006)
7. M. Nishizawa, C.R. Martin, V.P. Menon, Science **268**, 700 (1995)
8. H. Daiguji, Y. Oka, K. Shirono, Nano Lett. **5**, 2274 (2005)
9. R. Fan, M. Yue, R. Karnik, A. Majumdar, P. Yang, Phys. Rev. Lett. **95**, 086607 (2005)
10. Z.S. Siwy, M.R. Powell, A. Petrov, E. Kalman, C. Trautmann, R.S. Eisenberg, Nano Lett. **6**, 1729 (2006)
11. Z.S. Siwy, Adv. Funct. Mater. **16**, 735 (2006)
12. H. Li, Y. Zheng, D. Akin, R. Bashir, J. Microelectromech. Syst. **14**, 103 (2005)
13. J.G. Kralj, M.T.W. Lis, M.A. Schmidt, K.F. Jensen, Anal. Chem. **78**, 5019 (2006)
14. J. Li, D. Stein, C. McMullan, D. Branton, M.J. Aziz, J.A. Golovchenko, Nature **412**, 166 (2001)
15. D. Stein, J. Li, J.A. Golovchenko, Phys. Rev. Lett. **89**, 276106 (2002)
16. A.J. Storm, J.H. Chen, X.S. Ling, H.W. Zandbergen, C. Dekker, Nat. Mater. **8**, 537 (2003)
17. C.L. Gardner, W. Nonner, R.S. Eisenberg, J. Comput. Electron. **3**, 25 (2004)
18. S.M. Sze, *Physics of Semiconductor Devices* (Wiley-Interscience, 1981)
19. R.S. Muller, T.I. Kamins, M. Chan, *Device Electronics for Integrated Circuits* (John Wiley and sons Inc., 2003)
20. J.D. Zhou, S.T. Cui, H.D. Cochran, Mol. Phys. **101a**, 1089 (2003)
21. R.M. Lynden-Bell, J. Rasaiah, J. Chem. Phys. **105**, 9266 (1996)
22. J.B. Heng, A. Aksimentiev, C. Ho, P. Marks, Y.V. Grinkova, S. Sligar, K. Schulten, G. Timp, Biophys. J. **90**, 1098 (2006)